Critical Capillary Waves of Biomolecular Condensates

Shunsuke F. Shimobayashi *
Center for iPS Cell Research and Application, Kyoto University, Sakyo-ku, Kyoto 606-8507, Japan

Paul J. Ackerman
Department of Chemical and Biological Engineering, Princeton University, Princeton, New Jersey 08544, USA

Tomo Kurimura
Center for iPS Cell Research and Application, Kyoto University, Sakyo-ku, Kyoto 606-8507, Japan

Takashi Taniguchi
Department of Chemical Science and Engineering, Kyoto University, Kyoto 615-8510, Japan

Clifford P. Brangwynne
Department of Chemical and Biological Engineering, Princeton University, Princeton, New Jersey 08544, USA;
Howard Hughes Medical Institute, Princeton University, Princeton, New Jersey 08544, USA;
and Omenn-Darling Bioengineering Institute, Princeton University, Princeton, New Jersey 08544, USA

(Received 1 December 2025; accepted 21 May 2026; published 25 June 2026)

Biomolecular condensates formed by phase separation are key players in cellular organization, yet their interfacial mechanics remain poorly understood. Here we show that both synthetic and endogenous nuclear condensates exhibit critical-like interfacial behaviors near the phase boundary, including enhanced capillary fluctuations and reduced surface tension. By combining optogenetic control with submicron-resolution fluctuation spectroscopy, we quantitatively estimate surface tension, bending rigidity, and effective viscosity. Surface tension diminishes as the system approaches the critical composition, consistent with classical theories of phase separation. Notably, bending elasticity emerges as an unexpected feature of these nuclear liquidlike structures, suggesting the formation of structured interfacial layers that progressively weaken near criticality. Among these condensates, the nucleolus displays exceptionally high viscosity, which may arise in part from viscoelastic coupling to the surrounding perinucleolar heterochromatin, effectively increasing the apparent viscosity in the long-time fluctuation regime. This noninvasive approach enables probing condensate mechanics in living cells and may provide a basis for diagnosing or modulating condensates in biomedical contexts.

DOI: 10.1103/8rgq-wymv

I. INTRODUCTION

Biomolecular condensates formed via liquid-liquid phase separation and related phase transitions have emerged as a fundamental mechanism for organizing the intracellular environment without membranes [1–6]. These dynamic compartments concentrate specific proteins and nucleic acids to facilitate diverse biological processes, including gene expression, RNA metabolism, and signal transduction. Importantly, aberrant condensate formation has been linked to a range of diseases, such as neurodegenerative disorders and cancers, highlighting the need to understand the physical principles governing their material properties [7–9]. Among these properties, surface tension plays a central role in defining condensate shape, stability, and dynamics, particularly during processes such as fusion or wetting [10,11]. Bending rigidity, typically considered irrelevant for liquidlike droplets, has recently been suggested to contribute to condensate morphology [12], raising the possibility that condensates possess unexpectedly complex interfacial mechanics.

Fluctuation spectroscopy (often termed flicker spectroscopy) has a long tradition in soft-matter physics and biophysics as a quantitative route from thermally driven shape undulations to interfacial mechanical parameters [13,14]. Classic theoretical analyses of erythrocyte flickering and subsequent developments established how mode-resolved fluctuation spectra encode effective surface tension and bending elasticity, and the framework has been extended to a broad range of soft interfaces, including synthetic lipid membranes [15,16], colloidal fluid-fluid interfaces [17], and, more recently, biomolecular condensates [12]. Here we apply flicker spectroscopy to quantify how condensate interfacial mechanics behave throughout the phase diagram, particularly near a critical point. Given that intracellular condensates are

*Contact author: s.shimobayashi@cira.kyoto-u.ac.jp

Published by the American Physical Society under the terms of the Creative Commons Attribution 4.0 International license. Further distribution of this work must maintain attribution to the author(s) and the published article's title, journal citation, and DOI.

inherently multicomponent nonequilibrium systems, it remains unclear whether their interfacial behavior near criticality conforms to theoretical expectations established for classical critical fluids [18].

II. RESULTS

A. Quantification of surface fluctuations and material properties of biomolecular condensates in living cells

To quantify the interface properties of condensates in living cells, we first examine a tractable optogenetic system, Corelets [3,19]. Corelets enable optogenetic control of phase separation in human osteosarcoma (U2OS) cells through light-activated oligomerization of proteins including the intrinsically disordered regions (IDRs) of FUS or HNRNPA1 (FUS_N, residues 1–214; $HNRNPA1_C$, residues 186–320), which are model aromatic-rich polar sequences [3,19] [Fig. 1(a)]. We activate optogenetic oligomerization and then record time-lapse images of the resulting condensates and detect the contours, clearly observing surface fluctuations with a velocity of approximately 10 nm/s [Figs. 1(b) and 1(c)]. We find that the time-averaged contours are generally not perfect circles [Fig. 1(b)], likely due to the inhomogeneous mechanical environment in living cells. In order to quantify the fluctuations in the condensate equatorial plane, we consider the contour deviation $\delta r(\varphi, \Delta t)$ with a polar angle φ and time lag Δt,

$$\delta r(\varphi, \Delta t) = r(\varphi, t + \Delta t) - r(\varphi, t), \tag{1}$$

where we set a polar coordinate system from the center of mass of each condensate [Fig. 1(b)]. To quantify these dynamics, the fluctuation amplitude $|\delta r(\varphi, \Delta t)|^2$ was first averaged over all time point pairs with the same Δt within a single condensate, yielding $\langle|\delta r(\varphi, \Delta t)|^2\rangle$, and then subsequently averaged over the angular coordinate φ to obtain $\langle|\delta r(\Delta t)|^2\rangle$. The approach to the plateau can be well described by a single exponential $\langle|\delta r(\Delta t)|^2\rangle \propto 1 - e^{-\Delta t/\Delta t_0}$, from which we determined relaxation times Δt_0 of 2.6 ± 1.3 s and 1.1 ± 0.1 s for FUS_N and $HNRNPA1_C$ Corelets, respectively [Fig. 1(d)]. Fourier decomposition of the experimentally measured contour difference $\delta r(\varphi, \Delta t)$ yields the mode-resolved fluctuation spectrum $\langle|\Delta A_m(\Delta t)|^2\rangle$, which appears later in Eq. (4), where $\Delta A_m(\Delta t)$ is defined as the Fourier coefficient of $\delta r(\varphi, \Delta t)$ for Fourier mode m.

To theoretically elucidate the fluctuation behavior, we model the free-energy functional of the condensate surfaces, which can be expressed as

$$F = \int_S \left(\gamma + \frac{\kappa}{2}H^2\right) dS, \tag{2}$$

where γ, κ, and H are the condensate surface tension, surface bending modulus, and surface local curvature, respectively [20]. The equation of motion of the condensate surface, under the overdamped local-friction approximation, is given by

$$\xi \frac{\partial r(\theta, \varphi, t)}{\partial t} = -\frac{\delta F}{\delta r} + n(\theta, \varphi, t), \tag{3}$$

where ξ is a friction coefficient and $n(\theta, \phi, t)$ is a noise term reflecting microscopic fluctuations (e.g., thermal noise) [21]. Assuming thermally driven surface fluctuations on the cross-sectional plane at $\theta = \pi/2$ in the spherical coordinate system (see Sec. I of the Supplemental Material [22] and Fig. S1 therein), the fluctuation spectrum $\langle|\Delta A_m(\Delta t)|^2\rangle$ can be expressed as (with $m = 2, 3, 4, \ldots$)

$$\langle|\Delta A_m(\Delta t)|^2\rangle = \sum_{n=1}^{\infty} \frac{2r_0^2 k_B T}{\mathcal{E}_{n+m}} \left[N_{n+m,m} P_{n+m}^m(0)\right]^2 \times \left[1 - \exp\left(-\mathcal{E}_{n+m}\Delta t / r_0^2 \xi\right)\right], \tag{4}$$

$$\mathcal{E}_\ell = [\ell(\ell+1) - 2]\left[\kappa \ell(\ell+1) + \gamma r_0^2\right]. \tag{5}$$

Here $N_{\ell,m} = \sqrt{\frac{2\ell+1}{4\pi}\frac{(\ell-m)!}{(\ell+m)!}}$ and P_ℓ^m is the associated Legendre polynomial. The parameters r_0, k_B, T, and ξ are the mean condensate radius in the equatorial plane, the Boltzmann constant, temperature, and friction coefficient, respectively. The parameters γ, κ, and ξ can be measured by fitting $\langle|\Delta A_m(\Delta t)|^2\rangle$ with Eq. (4). For our fit, modes ($m \geqslant 15$) were excluded because the analysis approaches the resolution limit of the method and the spectra are increasingly affected by measurement noise, though still above the noise floor [16].

Figure 1(e) shows the representative fluctuation spectrum for a single condensate of FUS_N Corelets over 500 frames at time lags $\Delta t = 0.06,\ 0.3,$ and 30 s with the best-fit lines obtained using Eq. (4). As shown in Fig. S2 in Ref. [22], the spectrum for $\Delta t = 30$ s can be considered as the $\Delta t \to \infty$ case for the Corelet system. In this limit, the spectrum can be fitted using the expression $\langle|\Delta A_m(\infty)|^2\rangle = \sum_{n=1}^{\infty} \frac{2r_0^2 k_B T}{\mathcal{E}_{n+m}} [N_{n+m,m} P_{n+m}^m(0)]^2$, yielding γ and κ [Fig. 1(e)]. The spectrum for $\Delta t < 30$ s was fitted by Eq. (4), where the values of γ and κ obtained from the previous fitting were substituted, to determine ξ. The identical analysis procedure was also applied to $HNRNPA1_C$ Corelets. The theoretical prediction, as shown by dashed lines, demonstrates that the κ contribution exhibits an m^{-3} scaling, while the γ contribution exhibits an m^{-1} scaling. Hence, the -2 power law, as experimentally observed, signifies a regime where both terms contribute concurrently. Moreover, Fig. 1(f) shows the fluctuation spectrum $\langle|\Delta A_m(\Delta t)|^2\rangle$ for a large set of individual FUS_N and $HNRNPA1_C$ condensates (500 frames, $\Delta t = 30$ s), exhibiting a power law with a slope of nearly -2 against m. Fitting yields statistical values for a bending rigidity κ ranging from $1k_BT$ to $10k_BT$, consistent with previous estimates for stress granules [12]. Surface tension γ ranges from 10^{-7} to 10^{-5} N/m, in alignment with previously reported values for both *in vitro* and *in vivo* condensates [11,12,23–25]. The extracted friction coefficient ξ spans from 10^{-3} to 10^{-2} N s/m; to our knowledge, this represents the first quantitative measurement of interfacial friction for intracellular condensates.

B. Quantification of surface fluctuations and material properties of endogenous nuclear condensates

Next we aimed to test the applicability of our approach to endogenous nuclear condensates, focusing on nucleoli (sites of ribosome biogenesis) and nuclear speckles, which serve as hubs for mRNA processing and splicing factors [11,26] [Fig. 2(a)]. As shown in Fig. 2(b), the two condensates exhibited distinct magnitudes and timescales of interfacial fluctuations. We computed the fluctuation spectra

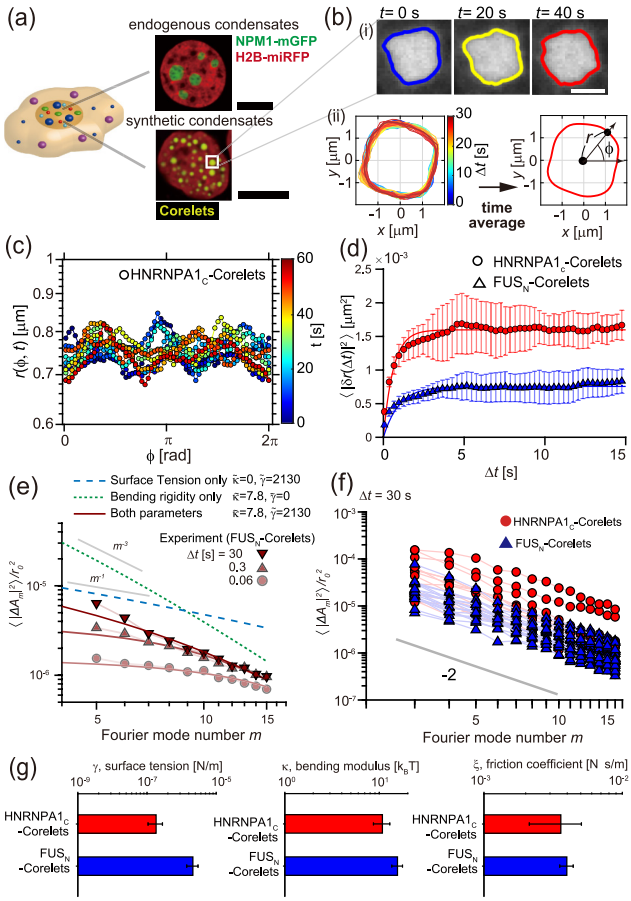

FIG. 1. Quantification of surface fluctuations and material properties of biomolecular condensates in living cells. (a) Confocal fluorescence images of U2OS cells expressing either NPM1-mGFP (nucleolar marker) and H2B-miRFP (chromatin/histone marker) or the optogenetic HNRNPA1$_C$-Corelet constructs (pHR-HNRNPA1$_C$-mCherry-sspb and pHR-NLS-iLID-EGFP-FTH1). The scale bar is 10 μm. (b) (i) Surface fluctuation of a single condensate of HNRNPA1$_C$ Corelets. The condensate interfaces are represented by the solid lines. The scale bar is 1 μm. (b) (ii) Overplots after centroid alignment and time average of contours of HNRNPA1$_C$ Corelets over 30 s (167 frames at a frame interval of $\Delta t = 180$ ms). The centroid is indicated by the black circle; $r(\varphi, t)$ denotes the radial distance of the contour from the centroid at polar angle φ. (c) Temporal dynamics of condensate contour $r(\varphi, t)$ for HNRNPA1$_C$ Corelets ($t = 0, 12, 24, 36, 48, 60$ s). (d) Ensemble average of the mean-square contour difference $\langle|\delta r(\Delta t)|^2\rangle$ as a function of lag time Δt for FUS$_N$ and HNRNPA1$_C$ Corelets. The solid lines show the best fit to $\langle|\delta r(\Delta t)|^2\rangle \propto 1 - e^{-\Delta t/\Delta t_0}$. (e) Normalized fluctuation spectrum $\langle|\Delta A_m(\Delta t)|^2\rangle/r_0^2$ of FUS$_N$ Corelets against the Fourier mode number m. The experimental data (symbols) are shown for different time lags ($\Delta t = 30$, 0.3, and 0.06 s). The solid lines represent the best fits to the data using Eq. (4). The dashed lines exhibit a power law with a slope of m^{-1} for the surface-tension-only model and m^{-3} for the bending-rigidity-only model. (f) Normalized fluctuation spectrum $\langle|\Delta A_m|^2\rangle/r_0^2$ against the Fourier mode number m with $\Delta t = 30$ s for FUS$_N$ ($n = 21$) and HNRNPA1$_C$ Corelets ($n = 14$). The gray line indicates an m^{-2} guide to the eye. (g) Box plots comparing surface tension γ (left), bending modulus κ (middle), and friction coefficient ξ (right), with red and blue boxes representing HNRNPA1$_C$ Corelets and FUS$_N$ Corelets, respectively. The error bars represent the standard error. Here n is the number of analyzed condensates.

$\langle|\Delta A_m(\Delta t)|^2\rangle$ with $\Delta t = 750$ s for nucleoli and $\Delta t = 250$ s for nuclear speckles, revealing a power-law decay with an exponent of -2 and confirming the presence of larger fluctuations in nuclear speckles [Fig. 2(c)]. To rule out experimental noise, we performed identical measurements after fixation with 4% paraformaldehyde, verifying that the observed fluctuation signals were well above the noise floor, particularly for long-wavelength modes (low m) (see Fig. S3 in Ref. [22]).

From these spectra, we determined the surface tension, bending modulus, friction coefficient, and effective viscosity as summarized in Fig. 2(d). The surface tension of nuclear condensates ranged from 10^{-7} to 10^{-6} N/m, consistent with prior measurements in HeLa cells and *Xenopus* oocytes [11,23], as well as colloid-polymer emulsions [17]. Strikingly, the bending modulus of these endogenous condensates again fell within $1k_BT$–$10k_BT$, suggesting that intracellular condensates—both nuclear and cytoplasmic, native and synthetic—may share similar levels of interfacial stiffness. Given the multicomponent nature of intracellular condensates, it is plausible that certain components preferentially accumulate at the interface, forming a compositionally distinct and structured layer. Such a layer may exhibit lateral molecular organization and cohesive interactions, akin to a Langmuir monolayer [10], thereby contributing to the observed bending rigidity of the interface. Supporting this notion, recent work on *Caenorhabditis elegans* P granules has demonstrated that MEG-3 forms low-dynamic protein clusters at the condensate interface to suppress coarsening and enhance structural integrity [27]. This picture is also consistent with recent *in vitro* reports of mesoscale protein clusters that likewise imply a structured interfacial layer [28]. These findings raise the possibility that membraneless organelles may exhibit membranelike mechanical properties due to surface-bound molecular scaffolds. Since our focus is on nuclear condensates, it is also tempting to speculate that such scaffolds could be provided by the surrounding chromatin matrix. However, their contribution would likely manifest in the apparent viscosity rather than in the bending rigidity, as our analysis probes long-time fluctuations beyond the relaxation regime. Notably, the nucleolus, despite being surrounded by perinucleolar heterochromatin, did not show a substantially higher κ than other nuclear condensates [Fig. 2(d)].

In contrast, nucleoli exhibited an anomalously high friction coefficient, over an order of magnitude greater than that of Corelet condensates and nuclear speckles [Fig. 2(d)]. Given that the low-mode regime is dominated by surface tension rather than elastic restoring forces and that viscous dissipation is expected to dominate over elastic losses, the friction coefficient ξ can be related to the effective viscosity η via $\xi \approx \eta r$ [21], where r denotes the condensate radius. Using the experimentally measured r, we can evaluate the effective viscosity, shown in a bar graph [Fig. 2(d)]. The effective viscosities we obtained for Corelet condensates and nuclear speckles are comparable to previously reported large-scale viscosities of the surrounding nucleoplasm (10^2–10^3 Pa s) measured by microrheology and magnetic bead experiments [29,30]. This is also approximately 1000 times higher than those of most *in vitro* condensates (approximately 1 Pa s), highlighting the highly viscous intracellular environment [24,25].

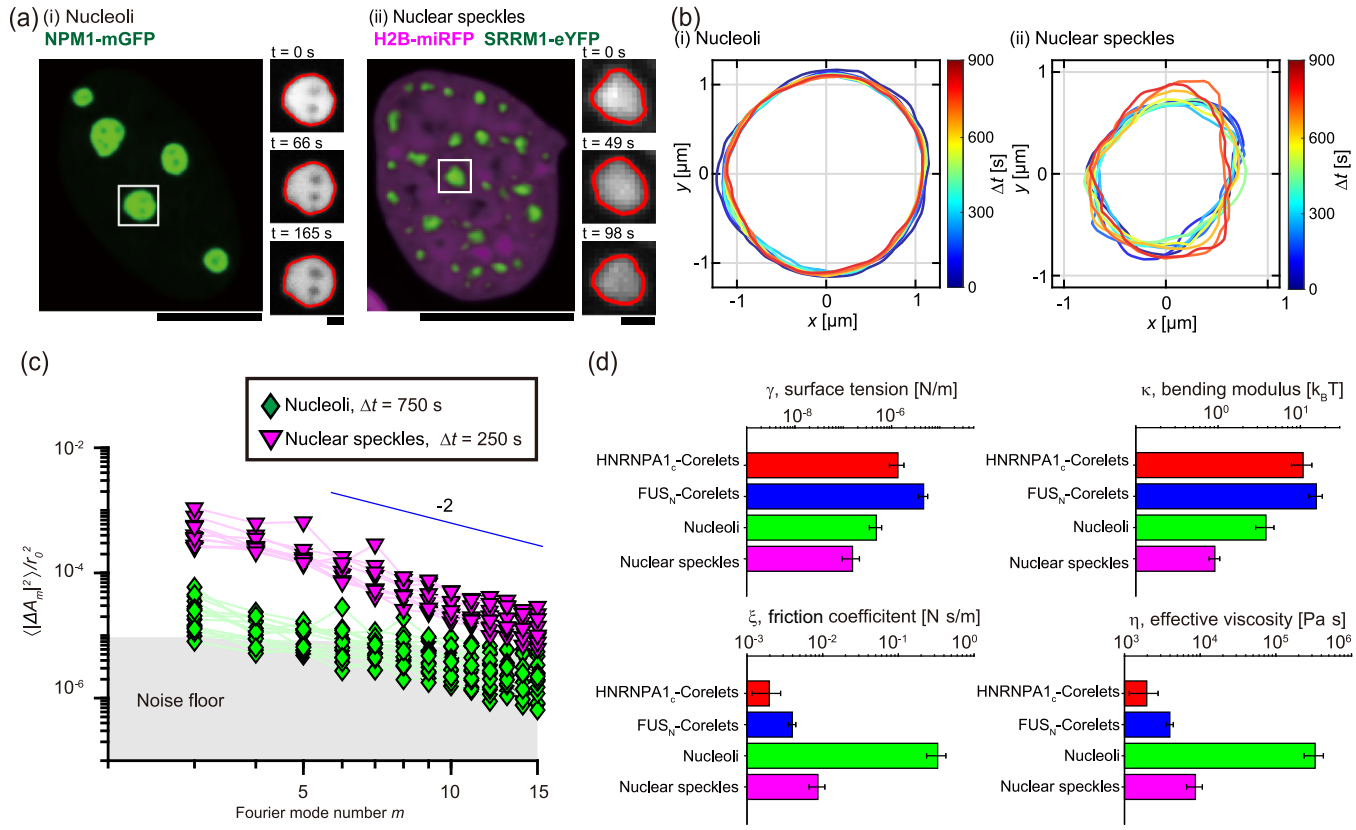

FIG. 2. Quantification of surface fluctuations and material properties of endogenous nuclear condensates. (a) Fluorescence images of U2OS cells expressing NPM1-mGFP (nucleolar marker) or expressing SRRM1-eYFP (nuclear speckle marker) and H2B-miRFP (chromatin/histone marker). Time-lapse confocal images of a single condensate are also displayed. The scale bar is 10 μm for large images and 1 μm for small images. (b) Overplots of a single condensate contour after centroid alignment of (i) nucleoli and (ii) nuclear speckles in U2OS cells with time lags $\Delta t = 30$ s (50 frames) and $\Delta t = 10$ s (50 frames), respectively. (c) Normalized fluctuation spectrum $\langle|\Delta A_m|^2\rangle/r_0^2$ against the Fourier mode index m with $\Delta t = 750$ s for nucleoli ($n = 15$) and $\Delta t = 250$ s for nuclear speckles ($n = 19$). The gray shaded area indicates the noise floor (estimated from fixed samples; see Fig. S3 in Ref. [22]). The blue line indicates an m^{-2} guide to the eye. (d) Bar graphs show the mean and standard error of surface tension γ, bending modulus κ, friction coefficients ξ, and effective viscosity η for HNRNPA1$_C$ Corelets ($n = 14$), FUS$_N$ Corelets ($n = 21$), nucleoli ($n = 15$), and nuclear speckles ($n = 19$), respectively. Here n is the number of analyzed condensates.

Notably, the viscosity of nucleoli reaches approximately 10^5 Pa s, which is about 100 times greater than that of the nucleoplasm. Such exceptionally high viscosity highlights the distinct physical state of the nucleolus among nuclear condensates, characterized by a highly dense, multiphase organization with RNA- and RNP-rich subcompartments [11,31,32], which is also reflected by their distinct refractive index [33]. However, the contribution of perinucleolar heterochromatin likely elevates the apparent viscosity: Any viscoelastic coupling from the surrounding chromatin $\eta \approx G\tau$, where G is the shear modulus and τ is the structural relaxation time, would be extracted as a viscous rather than an elastic component in the long-time regime [34]. For comparison, previous studies that measured nucleoli from *Xenopus* oocytes reported viscosities on the order of 10^2–10^3 Pa s based on fusion dynamics [11] and micropipette aspiration [35]. Those are about two orders of magnitude lower than the effective viscosity we estimated for nucleoli, possibly because these amphibian germinal vesicle nucleoli lack the surrounding perinucleolar heterochromatin.

C. Analysis of critical capillary waves in synthetic versus endogenous condensates

To gain further physical insights into the material properties of condensates, we leveraged controllable optogenetics to explore their critical behavior. By decreasing blue-light intensity, we moved the Corelet system along a previously quantified phase diagram toward the critical composition [3], i.e., $\chi \to \chi_c$ and $C_{\rm dil}/C_{\rm den} \to 1$ [Fig. 3(a)], where χ denotes the Flory-Huggins interaction parameter, and $C_{\rm dil}$ and $C_{\rm den}$ denote the dilute- and dense-phase core concentrations, respectively. In our prior work, the phase diagram as a function of core concentration and the core-to-IDR ratio was measured and a critical core-to-IDR ratio was identified; here we use the concentration contrast $C_{\rm dil}/C_{\rm den}$ as an operational proxy for proximity to the critical regime (approaching unity). In particular, the Flory-Huggins theory predicts that surface tension vanishes at the critical point [36]. Consistent with this, we observed a marked increase in surface fluctuations near the critical point [Figs. 3(b) and 3(c)], reflecting enhanced capillary fluctuations [17]. By fitting the fluctuation

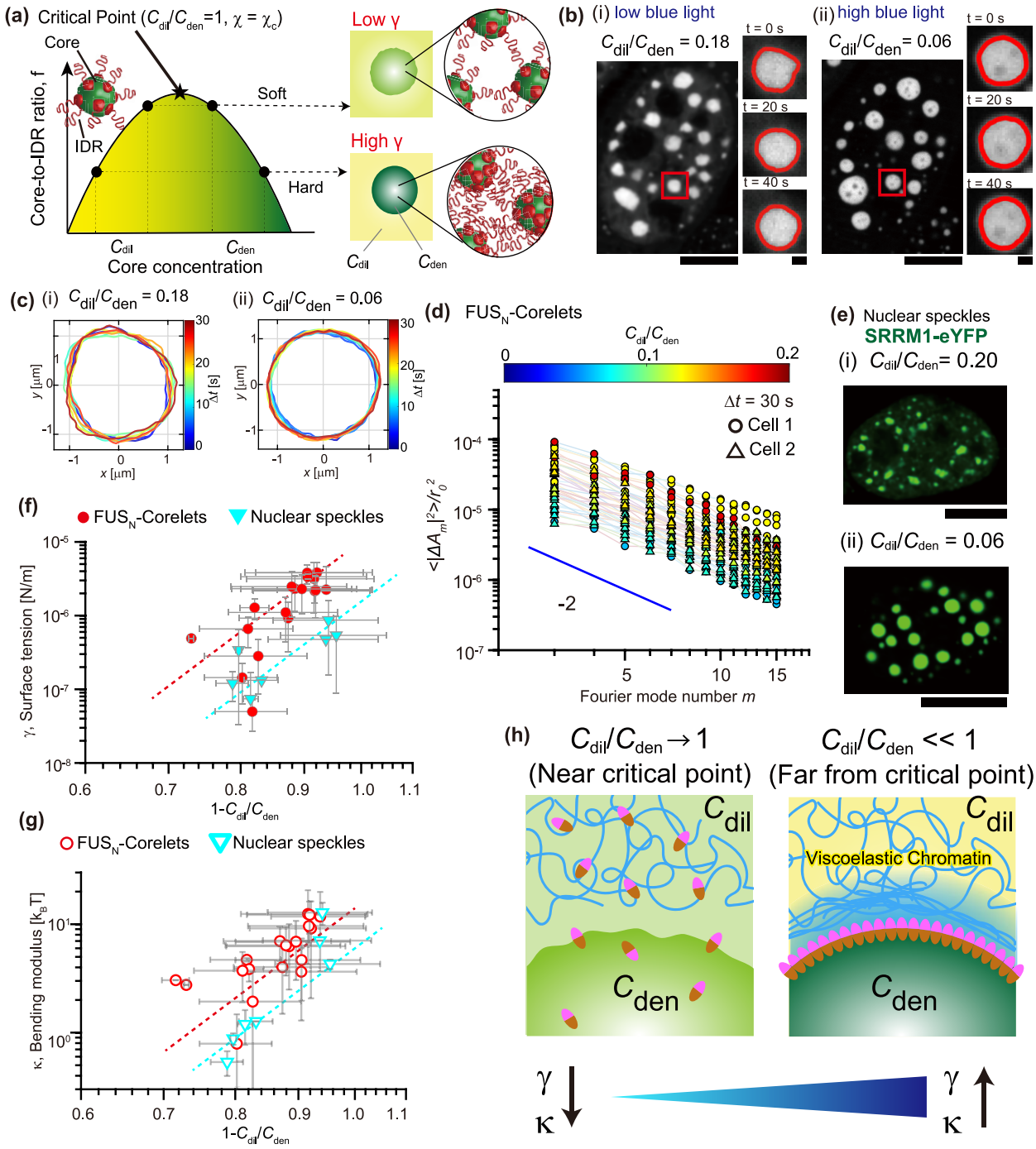

FIG. 3. Analysis of critical capillary waves in synthetic versus endogenous condensates. (a) Schematic of a phase diagram of the Corelet system, adapted from the phase diagram quantification in Ref. [3], showing that the surface tension γ decreases as a cell approaches the critical point, where $\chi = \chi_c$ and $C_{dil}/C_{den} = 1$. (b) Fluorescence images of U2OS cells expressing FUS$_N$ Corelets subjected to approximately (i) 10^{-4} W/cm^2 and (ii) 10^{-2} W/cm^2 intensities of blue light. Lower blue-light intensity drives the system closer to the critical point by bringing the concentration ratio C_{dil}/C_{den} closer to unity. The scale bar is 10 μm. Time-lapse confocal images of a single condensate are also displayed. The scale bar is 1 μm. (c) Overplots of single condensate contours in U2OS cells expressing FUS$_N$ Corelets under approximately (i) 10^{-4} W/cm^2 and (ii) 10^{-2} W/cm^2 intensities of blue light with a time lag $\Delta t = 180$ ms over 30 s after centroid alignment. (d) Normalized fluctuation spectrum $\langle|\Delta A_m(\Delta t)|^2\rangle/r_0^2$ against the Fourier mode index m with a time lag $\Delta t = 30$ s and various ratios C_{dil}/C_{den} for U2OS cells expressing FUS$_N$ Corelets ($n = 60$). Symbols denote two representative cells (○, cell 1; △, cell 2); color indicates C_{dil}/C_{den}. The blue line indicates an m^{-2} guide to the eye. (e) Fluorescence images of U2OS cells expressing different levels of SRRM1-eYFP, shown at (i) $C_{dil}/C_{den} = 0.20$ and (ii) $C_{dil}/C_{den} = 0.06$. (f) and (g) Surface tension γ and bending modulus κ plotted against $1 - C_{dil}/C_{den}$ for FUS$_N$ Corelets (103 condensates from 19 cells) and nuclear speckles (49 condensates from 13 cells). Data points represent single-cell means; error bars indicate standard deviations. The dashed lines are guides to the eye. (h) Schematic illustration of condensate interfaces far from (right) and closer to (left) criticality, parametrized by the concentration contrast C_{dil}/C_{den}.

spectra $\langle|\Delta A_m(\Delta t)|^2\rangle$, we quantified γ and κ across a range of concentration ratios. Consistent with theoretical expectations, surface tension decreased as $C_{\mathrm{dil}}/C_{\mathrm{den}} \to 1$ [Fig. 3(f)]. In contrast, the bending rigidity also decreased [Fig. 3(g)], but this behavior likely reflects structural changes at the interface, such as the loss of interfacial organization or adsorption, rather than a universal critical behavior.

To assess whether similar critical-like behavior exists in endogenous condensates, we overexpressed SRRM1, i.e., a scaffold protein of nuclear speckles, beyond its native levels. This led to more spherical speckles [Fig. 3(e)], lower $C_{\mathrm{dil}}/C_{\mathrm{den}}$, and reduced interfacial fluctuations, accompanied by a clear increase in surface tension and bending rigidity [Figs. 3(f) and 3(g)]. Despite the complex composition of endogenous condensates, surface tension exhibited similar critical-like behavior to synthetic systems [Fig. 3(f)], reinforcing the view that critical phenomena underlie both classes.

III. DISCUSSION AND PERSPECTIVE

Our findings reveal that nuclear condensates exhibit critical-like interfacial behavior, including the vanishing of surface tension near the phase boundary, consistent with classical theories of phase transitions. Beyond surface tension, our fluctuation spectroscopy uncovered bending rigidity as an unexpectedly prominent feature of these nominally liquidlike structures, suggesting the presence of structured interfacial layers stabilized by preferential adsorption or lateral organization of specific molecular components. Bending rigidity progressively decreased as the system approached criticality [Figs. 3(g) and 3(h)], likely reflecting the loss of such interfacial structure. In related work, similar fluctuation-based approaches have been implemented in a high-throughput manner by Law *et al.* [12]. In stress granules under various perturbations, they demonstrated that the measured fluctuation spectra cannot be captured by surface tension alone and require an additional bending-rigidity term, and they reported characteristic ranges of surface tension γ (sub-μN/m to a few μN/m) and bending rigidity κ (on the order of $k_{\mathrm{B}}T$). These values are comparable to those observed here, underscoring that $O(k_{\mathrm{B}}T)$ bendinglike contributions are likely a general feature of biomolecular condensates. Our study extends the fluctuation-spectroscopy framework by applying it across multiple endogenous nuclear condensates (nucleoli and nuclear speckles) as well as optogenetically induced synthetic condensates (Corelets) over a broad range of concentration contrasts.

While the discussion above focuses on interfacial properties inferred from plateau spectra at long lag times, our mode-resolved relaxation analysis using time-lagged statistics of mode dynamics reveals striking variations in effective viscosity: Most nuclear condensates exhibited values of 10^2–10^3 Pa s, whereas the nucleolus reached approximately 10^5 Pa s, possibly reflecting viscoelastic coupling to the surrounding perinucleolar heterochromatin. Notably, because the nucleolus is multiphase (FC/DFC/GC), internal interfacial slip and internal shear between subphases (e.g., DFC-GC) can, in principle, couple to outer shape relaxation and contribute to the inferred friction, alongside drag at the nucleolus-nucleoplasm interface. Related studies analyzed nucleolar coalescence kinetics in living cells and attributed the dynamics to dissipation in the surrounding nucleoplasm, thereby estimating nucleoplasmic viscosity [23]. In contrast, more recent micropipette-aspiration measurements have provided a direct assessment of the nucleolus's multiphase, compartment-specific viscoelasticity under near-native conditions [35]. Our approach is complementary to these studies in that we infer an effective condensate viscosity from mode-resolved relaxation, adding a fluctuation-based dynamical readout to the *in vivo* toolkit for probing condensate rheology.

Taken together, our study integrates optogenetic control with noninvasive fluctuation spectroscopy to quantify the material properties of condensates, including surface tension, bending rigidity, and viscosity, across synthetic and endogenous contexts. The ability to resolve these parameters at the submicron scale opens new opportunities to relate condensate material properties to biological function and dysfunction, enabling biophysical probing of pathological condensates through their intrinsic fluctuations and informing rational strategies to target aberrant phase behavior.

ACKNOWLEDGMENTS

We wish to acknowledge Kota Konishi, Akira Miyaki, Nguyen Thai Le, and Masumi Sanada for experimental and analytical support. This work was supported in part by JST, PRESTO Grant No. JPMJPR21E8 (to S.F.S.), JST FOREST Program, Grant No. JPMJFR230V (to S.F.S.); JSPS KAKENHI Grants No. 18K13521, No. 23K13072, and No. 25H01328 (to S.F.S.); research grants from iPS Cell Research Fund (to S.F.S.); the Uehara Memorial Foundation (to S.F.S.), Nakatani Foundation for Advancement of Measuring Technologies in Biomedical Engineering (to S.F.S.); The Kao Foundation for Arts and Sciences (to S.F.S.); 2022 iPS Academia Japan Grant (to S.F.S.), AFOSR MURI grant (to C.P.B.); and Princeton MRSEC (to C.P.B.).

S.F.S., T.T., and C.P.B. designed the research; S.F.S. and P.J.A. developed the analysis codes; S.F.S. performed the experiments; S.F.S. and T.K. analyzed the experimental and numerical data; S.F.S. wrote the manuscript; and S.F.S., P.J.A., T.T., T.K., and C.P.B. reviewed and edited the draft.

DATA AVAILABILITY

The data that support the findings of this article are not publicly available upon publication because it is not technically feasible and/or the cost of preparing, depositing, and hosting the data would be prohibitive within the terms of this research project. The data are available from the authors upon reasonable request.

[1] C. P. Brangwynne, C. R. Eckmann, D. S. Courson, A. Rybarska, C. Hoege, J. Gharakhani, F. Jülicher, and A. A. Hyman, Germline P granules are liquid droplets that localize by controlled dissolution/condensation, Science **324**, 1729 (2009).

[2] M.-T. Wei, Y.-C. Chang, S. F. Shimobayashi, Y. Shin, A. R. Strom, and C. P. Brangwynne, Nucleated transcriptional condensates amplify gene expression, Nat. Cell Biol. **22**, 1187 (2020).

[3] S. F. Shimobayashi, P. Ronceray, D. W. Sanders, M. P. Haataja, and C. P. Brangwynne, Nucleation landscape of biomolecular condensates, Nature (London) **599**, 503 (2021).

[4] X. Su, J. A. Ditlev, E. Hui, W. Xing, S. Banjade, J. Okrut, D. S. King, J. Taunton, M. K. Rosen, and R. D. Vale, Phase separation of signaling molecules promotes T cell receptor signal transduction, Science **352**, 595 (2016).

[5] S. F. Banani, H. O. Lee, A. A. Hyman, and M. K. Rosen, Biomolecular condensates: Organizers of cellular biochemistry, Nat. Rev. Mol. Cell Biol. **18**, 285 (2017).

[6] M. Yanagawa and S. F. Shimobayashi, Multi-dimensional condensation of intracellular biomolecules, J. Biochem. **175**, 179 (2024).

[7] A. Patel, H. O. Lee, L. Jawerth, S. Maharana, M. Jahnel, M. Y. Hein, S. Stoynov, J. Mahamid, S. Saha, T. M. Franzmann, *et al.*, A liquid-to-solid phase transition of the ALS protein FUS accelerated by disease mutation, Cell **162**, 1066 (2015).

[8] A. Boija, I. A. Klein, and R. A. Young, Biomolecular condensates and cancer, Cancer Cell **39**, 174 (2021).

[9] Y. Zhang, I. Stöppelkamp, P. Fernandez-Pernas, M. Allram, M. Charman, A. P. Magalhaes, M. Piedavent-Salomon, G. Sommer, Y.-C. Sung, K. Meyer, *et al.*, Probing condensate microenvironments with a micropeptide killswitch, Nature (London) **643**, 1107 (2025).

[10] S. A. Safran, *Statistical Thermodynamics of Surfaces, Interfaces, and Membranes* (Westview, Boulder, 1994).

[11] C. P. Brangwynne, T. J. Mitchison, and A. A. Hyman, Active liquid-like behavior of nucleoli determines their size and shape in *Xenopus laevis* oocytes, Proc. Natl. Acad. Sci. USA **108**, 4334 (2011).

[12] J. O. Law, C. M. Jones, T. Stevenson, T. A. Williamson, M. S. Turner, H. Kusumaatmaja, and S. N. Grellscheid, A bending rigidity parameter for stress granule condensates, Sci. Adv. **9**, eadg0432 (2023).

[13] F. Brochard and J. Lennon, Frequency spectrum of the flicker phenomenon in erythrocytes, J. Phys. (Paris) **36**, 1035 (1975).

[14] K. Fricke, K. Wirthensohn, R. Laxhuber, and E. Sackmann, Flicker spectroscopy of erythrocytes: A sensitive method to study subtle changes of membrane bending stiffness, Eur. Biophys. J. **14**, 67 (1986).

[15] J. Pécréaux, H.-G. Döbereiner, J. Prost, J.-F. Joanny, and P. Bassereau, Refined contour analysis of giant unilamellar vesicles, Eur. Phys. J. E **13**, 277 (2004).

[16] S. F. Shimobayashi, B. M. Mognetti, L. Parolini, D. Orsi, P. Cicuta, and L. Di Michele, Direct measurement of DNA-mediated adhesion between lipid bilayers, Phys. Chem. Chem. Phys. **17**, 15615 (2015).

[17] D. G. Aarts, M. Schmidt, and H. N. Lekkerkerker, Direct visual observation of thermal capillary waves, Science **304**, 847 (2004).

[18] P. C. Hohenberg and B. I. Halperin, Theory of dynamic critical phenomena, Rev. Mod. Phys. **49**, 435 (1977).

[19] D. Bracha, M. T. Walls, M.-T. Wei, L. Zhu, M. Kurian, J. L. Avalos, J. E. Toettcher, and C. P. Brangwynne, Mapping local and global liquid phase behavior in living cells using photo-oligomerizable seeds, Cell **175**, 1467 (2018).

[20] W. Helfrich, Elastic properties of lipid bilayers: Theory and possible experiments, Z. Naturforsch. C **28**, 693 (1973).

[21] U. Seifert, Configurations of fluid membranes and vesicles, Adv. Phys. **46**, 13 (1997).

[22] See Supplemental Material at http://link.aps.org/supplemental/10.1103/8rgq-wymv for additional experimental details, theoretical derivations, fitting procedures, and supplementary figures, which includes Ref. [37].

[23] C. M. Caragine, S. C. Haley, and A. Zidovska, Surface fluctuations and coalescence of nucleolar droplets in the human cell nucleus, Phys. Rev. Lett. **121**, 148101 (2018).

[24] H. Wang, F. M. Kelley, D. Milovanovic, B. S. Schuster, and Z. Shi, Surface tension and viscosity of protein condensates quantified by micropipette aspiration, Biophys. Rep. **1**, 100011 (2021).

[25] L. M. Jawerth, M. Ijavi, M. Ruer, S. Saha, M. Jahnel, A. A. Hyman, F. Jülicher, and E. Fischer-Friedrich, Salt-dependent rheology and surface tension of protein condensates using optical traps, Phys. Rev. Lett. **121**, 258101 (2018).

[26] A. I. Lamond and D. L. Spector, Nuclear speckles: A model for nuclear organelles, Nat. Rev. Mol. Cell Biol. **4**, 605 (2003).

[27] A. W. Folkmann, A. Putnam, C. F. Lee, and G. Seydoux, Regulation of biomolecular condensates by interfacial protein clusters, Science **373**, 1218 (2021).

[28] G. Golani, M. Seal, M. Kar, A. A. Hyman, D. Goldfarb, and S. Safran, Mesoscale properties of protein clusters determine the size and nature of liquid-liquid phase separation (LLPS), Commun. Phys. **8**, 226 (2025).

[29] A. Celedon, C. M. Hale, and D. Wirtz, Magnetic manipulation of nanorods in the nucleus of living cells, Biophys. J. **101**, 1880 (2011).

[30] A. H. De Vries, B. E. Krenn, R. Van Driel, V. Subramaniam, and J. S. Kanger, Direct observation of nanomechanical properties of chromatin in living cells, Nano Lett. **7**, 1424 (2007).

[31] M. Feric, N. Vaidya, T. S. Harmon, D. M. Mitrea, L. Zhu, T. M. Richardson, R. W. Kriwacki, R. V. Pappu, and C. P. Brangwynne, Coexisting liquid phases underlie nucleolar subcompartments, Cell **165**, 1686 (2016).

[32] D. L. Lafontaine, J. A. Riback, R. Bascetin, and C. P. Brangwynne, The nucleolus as a multiphase liquid condensate, Nat. Rev. Mol. Cell Biol. **22**, 165 (2021).

[33] T. Kim, J. Yoo, S. Do, D. S. Hwang, Y. Park, and Y. Shin, RNA-mediated demixing transition of low-density condensates, Nat. Commun. **14**, 2425 (2023).

[34] R. G. Larson, *Constitutive Equations for Polymer Melts and Solutions*, Butterworths series in chemical engineering (Butterworth-Heinemann, London, 2013).

[35] H. H. Cheng, J. V. Roggeveen, H. Wang, H. A. Stone, Z. Shi, and C. P. Brangwynne, Micropipette aspiration reveals differential RNA-dependent viscoelasticity of nucleolar subcompartments, Proc. Natl. Acad. Sci. USA **122**, e2407423122 (2025).

[36] A. Onuki, *Phase Transition Dynamics* (Cambridge University Press, Cambridge, 2002).

[37] S. F. Shimobayashi, M. Ichikawa, and T. Taniguchi, Direct observations of transition dynamics from macro- to micro-phase separation in asymmetric lipid bilayers induced by externally added glycolipids, Europhys. Lett. **113**, 56005 (2016).